Geomechanics and Engineering, *Vol. 43, No. 5 (2025) 343-358*
https://doi.org/10.12989/gae.2025.43.5.343

Experimental study on the synergistic reinforcement of silt using EICP and magnesium oxide

Bao min Liu[1a], Wan juan He[1b], Lin xian Gong*[1] and Yan Xu[2c]

[1]*Institute of Resource and Environment, Henan Polytechnic University, Jiaozuo, Henan 454000, China*
[2]*Construction Engineering College, Jilin University, Xin Min Zhu Street, Changchun, Jilin 130026, China*

(*Received October 26, 2024, Revised September 14, 2025, Accepted November 5, 2025*)

Abstract. In response to the challenges of high silt content, poor cohesion, and loose structure in the Yellow River floodplain, this study proposes a combined reinforcement method using enzyme-induced carbonate precipitation (EICP) and MgO to enhance mechanical properties. By adjusting the cementation solution concentration and MgO amount, the mechanical characteristics of the reinforced silt were systematically analyzed, and the reinforcement mechanism was thoroughly investigated. Results show that while cementation solution concentration significantly affects calcium carbonate precipitation during EICP, excessively high concentrations inhibit urease activity. The addition of MgO promotes magnesium carbonate hydroxide formation, improving mechanical properties and increasing unconfined compressive strength to a maximum of 5000 kPa, with distinct brittle failure characteristics. Residual strength, elastic modulus, and peak strength also improved. Although MgO delays flocculation and precipitation processes, it increases carbonate production. SEM and XRD analyses reveal that increasing cementation solution concentration and MgO content reduces inter-particle porosity and enhances soil microstructural stability. Overall, the combined EICP–MgO method shows exceptional strength improvement in silt, highlighting its practical applicability and innovative advantage over EICP alone.

Keywords: bio-cementation; enzyme-induced carbonate precipitation; ground improvement; MgO; silt

1. Introduction

Due to concentrated rainfall, the Yellow River Basin in China frequently experiences flood disasters, leading to repeated breaches and changes in the river course, forming large flood prone and silt deposition areas, known as the Yellow River floodplain. The Yellow River carries large amounts of silt from the upstream to the downstream, depositing it to form silt with unique characteristics in the floodplain area. Compared to regular silt, the silt in the Yellow River floodplain exhibits higher silt content, poor gradation, high particle roundness, and is difficult to compact. These characteristics contribute to frequent issues in road engineering within the region, severely affecting the construction and maintenance of roadbeds (Jin *et al.* 2020).

Traditional silt reinforcement methods can be broadly categorized into physical reinforcement and chemical reinforcement (DeJong *et al.* 2010, Tao *et al.* 2015, Wang *et al.* 2016). Physical reinforcement typically involves mechanical means such as compaction or dynamic compaction (Li *et al.* 2011), or the incorporation of fiber reinforcement materials into the soil (Khattak and Alrashidi 2006, Harianto *et al.* 2008). While these methods do not alter the fundamental physical and chemical properties of the soil or produce new chemical reaction products, they have limitations such as high costs and unstable reinforcement effects (Huang 2020). In contrast, chemical reinforcement involves the addition of additives (such as cement or polymers) that react with the soil minerals (Rodriguez-Navarro *et al.* 2002, Morales *et al.* 2019, Terzis and Laloui 2019), thereby improving the engineering properties of the soil. Chemical reinforcement has been widely adopted due to its relatively low cost, simple construction, and significant strength enhancement. However, for silts with high fine particle content and low clay content, traditional inorganic stabilizers often result in issues such as low early strength, high shrinkage, cracking, and poor long term stability. Moreover, traditional stabilizers may disrupt the soil's pH balance, leading to mineral loss, damage to vegetation, and contamination of groundwater systems, which contradict the principles of sustainable development (Achal and Mukherjee 2015). Therefore, there is an urgent need for an environmentally friendly and economical silt improvement technology.

Enzyme-induced calcium carbonate precipitation (EICP) technology is an emerging, eco-friendly soil stabilization technique that has been extensively studied in recent years in various fields, including pollutant immobilization, ground improvement, soil improvement, sealing of rock fissures, and dust suppression (Kavazanjian Jr *et al.* 2017, He *et al.* 2021, Liu *et al.* 2021, Zhu *et al.* 2022, Payan *et al.* 2024). In the standard EICP process, urea is hydrolyzed by urease to generate carbonate ions, which then react with Ca^{2+} from $CaCl_2$ to precipitate $CaCO_3$. Compared to

*Corresponding author, Ph.D.
E-mail: gonglx@hpu.edu.cn
[a]Assistant Professor
[b]Graduate Student
[c]Professor

ISSN: 2005-307X (Print), 2092-6219 (Online)

microbially induced calcium carbonate precipitation (MICP) technology (DeJong *et al.* 2006), EICP offers distinct advantages (Khoshdel Sangdeh *et al.* 2024). First, urease derived from plant sources can be directly extracted from plants, providing a stable source of highly active urease without the need for complex bacterial cultivation, thus resolving the issue of uncontrollable enzyme activity (Ran *et al.* 2015, Wu *et al.* 2020). Second, the nano-scale size of urease makes it more suitable for reinforcing fine-grained soils, such as silt from the Yellow River floodplain (Yin *et al.* 2019). Additionally, free urease is easily degradable and does not pose long-term environmental impacts (Kavazanjian and Hamdan 2015). However, when reinforcing soil using EICP, most of the urease exists in a free state and lacks nucleation sites necessary for calcium carbonate precipitation, resulting in smaller and more dispersed calcium carbonate crystals, which limits the overall reinforcement effect. Consequently, the effectiveness of EICP is slightly weaker compared to MICP (Nafisi *et al.* 2019, Song *et al.* 2020). To improve the reinforcement effect of EICP, researchers have attempted to combine it with other materials such as slag powder (Qi *et al.* 2022), Magnesium chloride (Putra *et al.* 2017), basalt fibers (Xiao *et al.* 2019), lignin (Zhang *et al.* 2022), skimmed milk powder (Almajed *et al.* 2019), and sodium-based montmorillonite (Yuan *et al.* 2022). Among the various additives investigated to enhance EICP performance, active MgO carbonation technology has gained particular attention because of its remarkable soil improvement capacity and environmental benefits (Yang *et al.* 2021). This technology leverages the carbonation process of MgO to reinforce soil, with the carbonation products not only filling voids but also exhibiting high strength and stiffness, while also facilitating the fixation of CO_2, offering significant ecological benefits (Vandeperre *et al.* 2008a, Unluer and Al-Tabbaa 2013, Liu and Chen 2015).

However, the primary limitation of using MgO for soil stabilization lies in the supply of carbon sources during the carbonation process (Dung *et al.* 2022). Although gaseous CO_2 can accelerate the carbonation reaction, it is challenging to obtain gaseous CO_2 for large-scale applications at construction sites. As a solution, some researchers have proposed combining microbially induced urea hydrolysis with MgO carbonation, using urea hydrolysis to provide the carbon source and promote the carbonation of MgO. Studies have shown that this combined technique offers advantages such as high curing strength, one-time formation, and wide adaptability (Yi *et al.* 2013; Huang *et al.* 2020; Chen *et al.* 2021; Yang *et al.* 2021; Wang *et al.* 2022). Another method for obtaining a carbon source involves utilizing plant-derived urease to catalyze urea hydrolysis, with the generated CO_3^{2-} being used for MgO carbonation. In this process, urease catalyzes the hydrolysis of urea, producing CO_3^{2-}, which infiltrate $Mg(OH)_2$ under certain pressure conditions and react to form different types of magnesium carbonate hydroxides. The carbonation products include hydromagnesite, fibrous magnesium carbonate, artinite, and nesquehonite (Vandeperre *et al.* 2008b). The reaction equation is shown as follows

$$MgO(s)+H_2O(l)\rightarrow Mg^{2+}(aq)+2OH^{-}(aq) \quad (1)$$

$$CO(NH_2)_2(aq)+2H_2O(l)\rightarrow 2NH^{4+}(aq)+CO_3^{2-}(aq) \quad (2)$$

$$Ca^{2+}(aq)+CO_3^{2-}(aq)\rightarrow CaCO_3(s) \quad (3)$$

$$Mg^{2+}(aq)+CO_3^{2-}(aq)+3H_2O(l)\rightarrow MgCO_3\bullet 3H_2O(s) \quad (4)$$

$$5Mg^{2+}(aq)+4CO_3^{2-}(aq)+4OH^{-}(aq)\cdot 4H_2O(l) \rightarrow (Mg_5(CO_3)_4(OH)_2\bullet 4H_2O)(s) \quad (5)$$

$$5Mg^{2+}(aq)+4CO_3^{2-}(aq)+2OH^{-}(aq)\cdot 5H_2O(l) \rightarrow (Mg_5(CO_3)_4(OH)_2\bullet 5H_2O)(s) \quad (6)$$

$$2Mg^{2+}(aq)+CO_3^{2-}(aq)+2OH^{-}(aq)\cdot 3H_2O \rightarrow (Mg_2(CO_3)(OH)_2\bullet 3H_2O)(s) \quad (7)$$

However, few studies have systematically investigated the combined use of EICP and MgO for reinforcing silt, particularly in the context of the Yellow River floodplain where high silt content and low cohesion pose major challenges. The lack of research on the synergistic mechanisms and practical applicability of this method constitutes the primary gap that the present study aims to address. This study employed the combined EICP and MgO technique to reinforce silt from the Yellow River floodplain. Through unconfined compressive strength tests, the effects of this combined reinforcement technique on the mechanical properties of silt were analyzed. In addition, by observing the reaction processes of EICP and EICP-MgO in both solution and silt, and utilizing tests such as scanning electron microscopy (SEM) and X-ray diffraction (XRD), the micro-mechanisms of reinforcement failure were thoroughly investigated. The results provide a novel eco-friendly approach for improving the silt in the Yellow River floodplain, demonstrating the potential of this method to enhance the mechanical properties of the silt.

2. Materials and methods

2.1 Materials

2.1.1 Silt from the Yellow River floodplain

The silt used in this study was collected from an ancient course of the Yellow River in Anyang, Henan Province, China, which is a typical silt from the Yellow River floodplain (Figs. 1(a) and (b)). Fig. 1(c) shows the particle size distribution curve of the Yellow River alluvial silt, based on experimental results. This silt has a relatively loose structure and low clay content. The coefficient of uniformity (Cu) of the silt is 3.33, and the coefficient of curvature (Cc) is 1.2, indicating that it is poorly graded silt. Laboratory tests further determined the basic physical properties of the silt (Table 1), and according to the soil classification standard GB/T 50145-2007 (Standard for Engineering Classification of Soil, China), this silt is classified as low liquid limit silt.

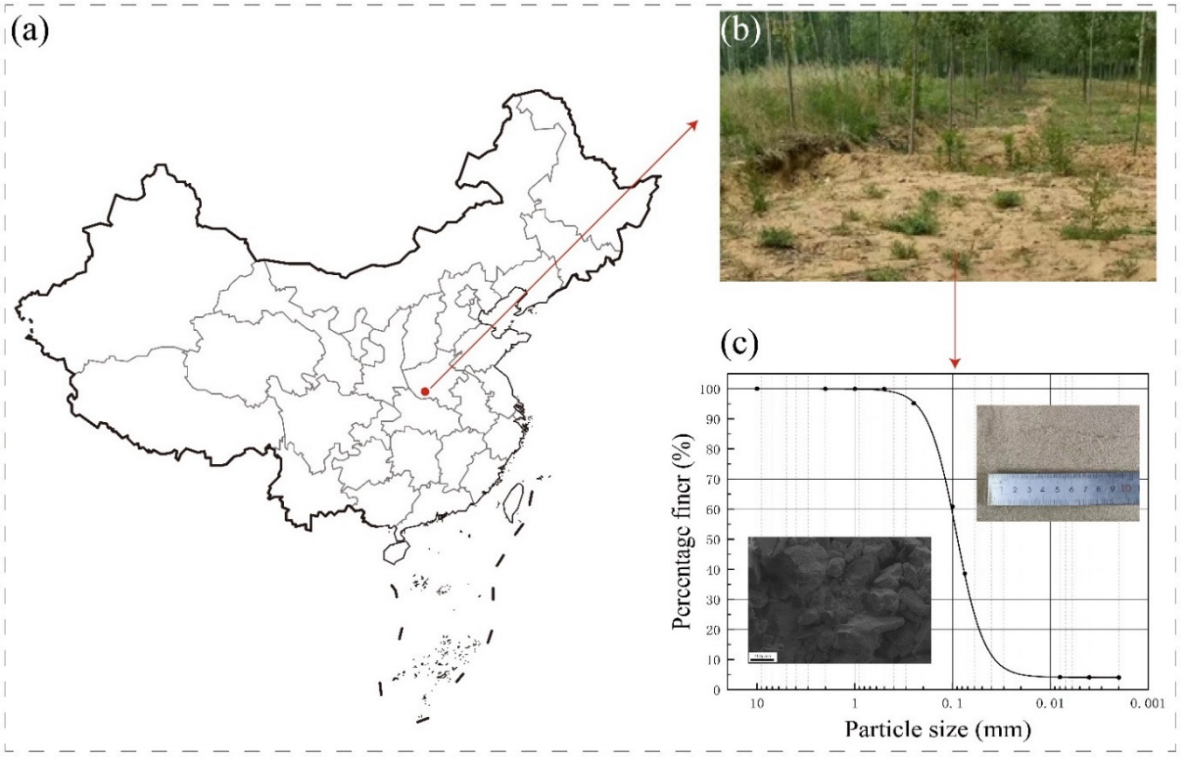

Fig. 1 Silt sample collection and characteristics: (a) Geographical location of silt sample collection, (b) Field sampling site for silt and (c) Silt particle size distribution

Table 1 Basic physical properties of silt in yellow plain area

Specific gravity Gs	Maximum dry density ρ_{dmax}	Natural water content %	Optimal water content %	Liquid limit W_L/%	Plastic limit W_P/%	Plasticity index I_P
2.91	1.68	15.43	16.07	25.11	18.00	7.11

2.1.2 Active MgO, Urease, and cementation solution

In this section, the activity of the MgO used in the tests is determined. A high-activity magnesium oxide produced by Israel's ICL company was employed, and its reactivity was evaluated using the standard hydration method (WB/T 1019–2002). First, the magnesium oxide sample was dried at 105°C for 24 hours, and the weight was recorded as M1. Then, 2 grams of the sample were placed in a beaker containing 20 milliliters of deionized water, covered with plastic wrap with small holes, and left in a constant temperature and humidity chamber at 20°C and 70% relative humidity for 24 hours. After the reaction, the sample was dried again to a constant weight and weighed, recorded as M2. The activity index of magnesium oxide, A, was calculated using the following formula

$$A = \frac{M_2 - M_1}{0.45M_1} \times 100\% \quad (8)$$

Where A represents the activity index of MgO, M_1 is the mass of the active MgO before hydration, and M_2 is the mass of the active MgO after hydration. The factor 0.45 corresponds to the theoretical mass gain ratio between MgO and H_2O in the hydration reaction. Based on the calculations, the activity of the MgO used in this experiment is 67.5%, indicating that this MgO has a high reactive activity.

For this study, soybeans were chosen as the source for urease extraction, with the specific process shown in Fig. 2. Soybeans were ground into powder, sieved, and mixed with distilled water at a ratio of 100 g/L, which has been shown in previous studies to provide stable urease activity (Yuan *et al.* 2022). After stirring and centrifugation, the supernatant (urease) was collected and mixed with the cementation solution (urease and $CaCl_2$) for soil reinforcement tests (Meng *et al.* 2021). Before use, the urease was mixed with urea at a 1:9 ratio to measure its average conductivity, resulting in an activity level of 8.3 m mol/L/min (Whiffin 2004, Whiffin *et al.* 2007, Gao *et al*. 2019, Shu *et al*. 2022). The cementation solution is a mixture of urea and calcium chloride, containing the reactants nitrogen and calcium for the EICP reaction. In this experiment, cementation solutions with concentrations of 1.0, 2.0, and 3.0 mol/L urea and equimolar $CaCl_2$ (1:1 molar ratio) were used.

2.2 Specimen preparation

Cylindrical specimens with a diameter of 40 mm and a length of 80 mm were prepared, consistent with standard

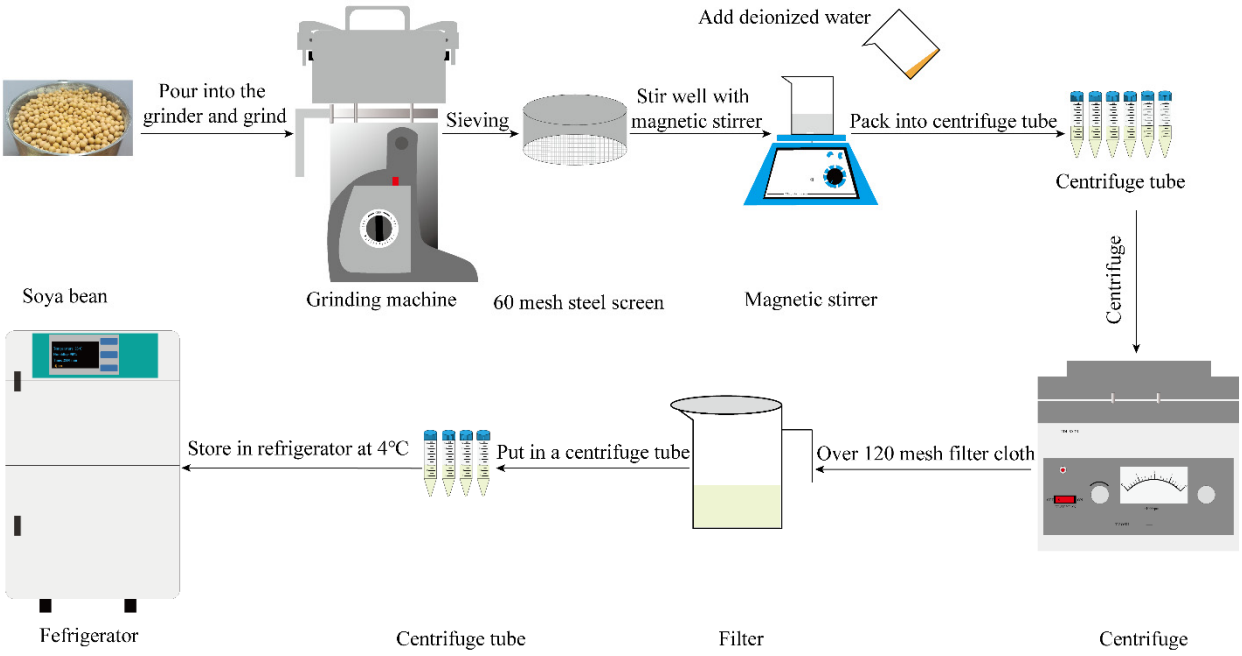

Fig. 2 The extraction procedure of crude enzyme (adapted from Gao *et al*. 2019, Shu *et al*. 2022)

UCS testing practice (ASTM D2166) and previous bio-cementation studies (Chen *et al.* 2023). The specimens for mechanical testing were prepared using polyvinyl chloride (PVC) cylindrical molds. The inner walls of the molds were coated with petroleum jelly, and a PVC soft film was inserted to facilitate specimen removal. A rubber plug, geotextile, and permeable stone were placed sequentially at the base of each mold to provide a flat bottom surface and prevent leakage of soybean urease and cementation solution during curing. The detailed preparation process is illustrated in Fig. 3.

To ensure specimen uniformity, a layered compaction method was employed (Ibraim *et al.* 2012). The Yellow River floodplain silt was first mixed thoroughly with MgO, after which urease and cementation solution were blended into the mixture. The mixture was divided into four equal portions by weight, each placed into the mold sequentially and compacted. The surface of each layer was roughened prior to adding the next to minimize interlayer discontinuities, the specimens were placed in a controlled chamber at 30°C for 24 h to allow stabilization before grouting. Grouting was then performed, followed by curing at 30°C for 7 days. After curing, the specimens were oven-dried at 105°C for 24 h until constant weight was achieved, yielding the final samples for UCS testing.

In this experiment, three groups of specimens were prepared, with a total of 16 samples. The specific grouping and grouting experiment plan are shown in Table 2. The experimental variables were the concentration of the cementation solution and the amount of MgO added. Specifically, one group consisted of untreated silt from the Yellow River floodplain, serving as the control group; the second group used different concentrations of the cementation solution for EICP reinforcement; and the third group combined various MgO dosages (6%, 12%, and 18% by dry soil mass) with the EICP treatment. The aim of the experiment was to explore and compare the differences in reinforcement effects between using only EICP and using the combined EICP-MgO treatment on silt. To ensure the comparability of the experiment, the relative density of all specimens was kept consistent, with the mass of the silt from the Yellow River floodplain used in each specimen being 167.5 g, and the specimen height controlled at 8 cm. The volume of cementation solution was controlled at 1.1 times the pore volume of the specimen to ensure full saturation.

Table 2 Grouting test plan and sample grouping

Test group	Cementation solution concentration (mol/L)	Urease dosage (ml)	MgO dosage (%)
C1	1	28.75	0
			6
			10
			14
			18
C2	2	28.75	0
			6
			10
			14
			18
C3	3	28.75	0
			6
			10
			14
			18

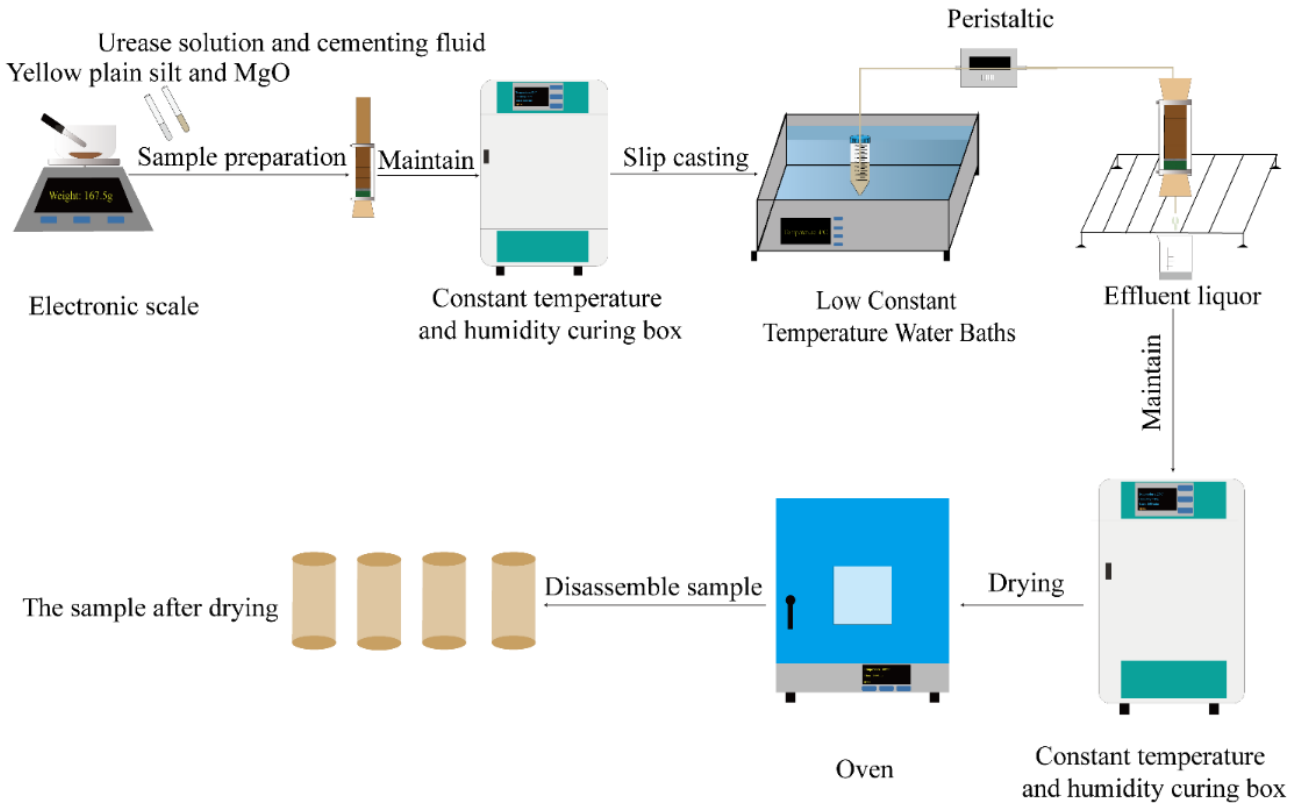

Fig. 3 Flow chart of experimental sample preparation

2.3 Tests

In this study, a series of laboratory tests were conducted to comprehensively evaluate the reinforcement mechanism of combining MgO with EICP. Unconfined compressive strength (UCS) tests were first performed to assess the influence of MgO dosage and cementation solution concentration on specimen strength and failure modes. To further clarify the reaction process, test tube experiments quantified the conversion efficiency of calcium carbonate and the additional carbonate formed with MgO. A flocculation test was then designed to measure flocculation time under different cementation solution concentrations and to evaluate the effect of MgO on precipitation behavior. Microscopic observations compared EICP products with and without MgO, while scanning electron microscopy (SEM) and X-ray diffraction (XRD) analyses characterized the microstructure and mineral composition. Together, these tests provide a systematic understanding of the macroscopic reinforcement effects and microscopic mechanisms of the combined EICP–MgO treatment.

2.3.1 Unconfined compression test

The unconfined compression test is a fundamental method for analyzing the mechanical properties of silt reinforced by EICP-MgO. In this study, the YYW-2 unconfined compression testing machine was used to conduct the unconfined compression tests. Before testing, the cured samples were carefully polished to a standard height of 8 cm, ensuring that both ends of the samples were flat to minimize experimental errors. During the test, the samples were compressed at a uniform loading rate of 0.6 mm/min until failure occurred. Throughout the process, the dial readings were continuously recorded, and the load was immediately removed after the sample failure. By analyzing the recorded stress-strain curves, the mechanical response of the reinforced silt can be thoroughly evaluated.

2.3.2 Carbonate content test

This study investigated the effects of reaction solution concentration and MgO incorporation on the EICP reaction through a series of carbonate content tests. The carbonate content tests were conducted on soil samples selected from portions of the specimens after the unconfined compression tests. The concentrations of the cementation solution were 1 mol/L, 2 mol/L, and 3 mol/L, respectively. To evaluate the impact of MgO on the EICP reaction, 2.01 g of MgO was selected for the experiment. The cementation solution concentrations used were 1 mol/L, 2 mol/L, and 3 mol/L, and the measured MgO was placed into three separate test tubes. The cementation solution and urease solution were then added dropwise into the test tubes, and the mixture was stirred with a glass rod to ensure a thorough reaction. After 24 hours, the amount of carbonate produced in the solutions under different cementation solution concentrations was measured. These tests will help in understanding the effects of reaction solution concentration and MgO on the EICP reaction.

(1) Calcium Carbonate Content Test

Weigh an untreated soil sample of the same mass and place it in a dried beaker. The soil sample is fully immersed in 0.1 mol/L hydrochloric acid (HCl) and left to react for one day

until the reaction is complete. Afterward, the sample is thoroughly rinsed with deionized water, and the beaker along with the sample is dried and weighed. The mass difference before and after the reaction represents the amount of calcium carbonate originally present in the soil sample. For the treated samples, a portion of the sample is weighed and placed in a dried beaker. The sample is fully immersed in 0.1 mol/L hydrochloric acid (HCl) and left to react for one day until the reaction is complete. Afterward, the sample is thoroughly rinsed with deionized water, and the beaker along with the sample is dried and weighed. The mass difference before and after the reaction represents the current amount of calcium carbonatein the sample. The increase in calcium carbonate mass in the treated sample compared to the original untreated sample represents the amount of calcium carbonate produced through EICP reinforcement. The calculation formula is as follows

$$M_3=M_4-M_5 \quad (9)$$

$$M_6=M_7-M_8 \quad (10)$$

$$M_9=M_6-M_3 \quad (11)$$

Where M_3 is the amount of calcium carbonate in the original soil sample; M_4 is the total mass of the original soil sample and the beaker; M_5 is the total mass of the soil sample and beaker after the reaction; M_6 is the current amount of calcium carbonate; M_7 is the total mass of the treated soil sample and the beaker; M_8 is the total mass of the treated soil sample and beaker after the reaction; and M_9 is the amount of calcium carbonate produced in the EICP reinforced sample.

(2) Chemical Conversion Efficiency

The chemical conversion efficiency is the ratio of the actual amount of calcium carbonate produced to the theoretically expected amount of calcium carbonate. The actual amount of calcium carbonate produced is the amount obtained from acid washing, denoted as M_9. The theoretically expected amount of calcium carbonate is the amount that would be produced if all the $CaCl_2$ in the injected cementation solution during the EICP process were completely converted into calcium carbonate. The calculation formula is as follows:

$$W=\frac{M_9}{M_{10}}\times 100\% \quad (12)$$

Where W is the chemical conversion efficiency; M_9 is the actual amount of calcium carbonate produced; and M_{10} is the theoretically expected amount of calcium carbonate produced.

(3) Carbonate Content Test

Since in the EICP-MgO reinforced silt samples, not only calcium carbonate precipitates are generated, but there is also unreacted MgO, as well as partially reacted $Mg(OH)_2$ and magnesium carbonate hydroxide that react with hydrochloric acid, the carbonate content in the samples cannot be directly measured using the acid-washing method. To test the carbonate content, the characteristic that both carbonates and hydrochloric acid produce CO_2 is utilized. Excess dilute hydrochloric acid is added to the reacted samples, and after acid-washing for one day, the mass is measured. The difference in mass between the sample before and after the reaction represents the lost CO_2, which corresponds to the carbonate content in the products. The fully reacted solution is poured into a pre-dried beaker, and the test tube is rinsed with a small amount of deionized water to ensure that all the carbonate adhering to the tube walls enters the beaker. The total mass of the solution and the beaker is then measured. Excess dilute hydrochloric acid is added to the beaker to ensure a complete reaction with the solution, and the mixture is slowly stirred with a glass rod to ensure thorough reaction. When no bubbles are generated in the solution, indicating that all the CO_2 has been released, the total mass of the solution and the beaker is measured again. The mass of the lost CO_2 can then be calculated. The calculation formula is as follows

$$M_{11}=M_{12}+M_{13}-M_{14} \quad (13)$$

Where M_{11} is the mass of CO_2; M_{12} is the total mass of the beaker and the solution before the addition of dilute hydrochloric acid; M_{13} is the mass of the dilute hydrochloric acid used; and M_{14} is the total mass of the beaker and the solution after acid washing.

Table 3 Test tube groups and required materials

Experimental grouping	MgO dosage (g)	Urease dosage (ml)	Cementation concentration (mol/L)
T0	0	5.75	1 2 3
T1	2.01	5.75	1 2 3

2.3.3 Test tube experiments

The test tube experiments allow for the exploration of the effects of different cementation solution concentrations and MgO addition on the flocculation time of the mixed solution. The experiments were conducted at a temperature of 30°C, with the solution mixtures in the test tubes prepared according to the ratios shown in Table 3. The ratio of urease solution to cementation solution was 1:1, and the test tubes were sealed with parafilm to prevent evaporation and external contamination. Images of the test tubes were taken at different time points after mixing the solutions to record the flocculation and sedimentation process. These recorded images allow for the analysis and comparison of the flocculation times under different conditions, providing further insights into the role of MgO in the EICP process. This method supports the understanding of the EICP reaction mechanism and helps to optimize experimental conditions.

2.3.4 Glass slide experiments

This study conducted three sets of glass slide experiments to observe the microscopic reactions of EICP and MgO in both solution and silt (Fig. 4). In the first set, silt was placed on a glass slide, and EICP solution was added dropwise until the silt was completely covered,

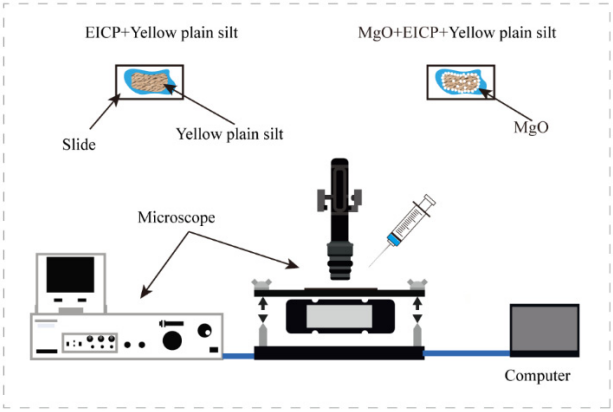

Fig. 4 Slide tests of EICP and EICP-MgO reinforced silt

allowing the EICP reaction process in the silt to be observed under a microscope. In the second set, EICP solution was added to a glass slide containing MgO, and the reaction between MgO and the EICP solution was observed. In the third set, a mixture of MgO and silt was evenly placed on a glass slide, and EICP solution was added dropwise until the solid particles were fully covered, with the microscope recording the reaction of EICP-MgO in the silt. It is important to note that, before the experiment begins, both the cementation solution and urease solution need to be vacuum-treated to prevent bubbles during microscopic observation, which could affect the experimental results and analysis.

2.3.5 Scanning electron microscope (SEM) test

The fractured specimens from the unconfined compression tests were selected for microscopic structural observation using a Quanta FEI 250 scanning electron microscope (SEM) produced by FEI, USA. Before the test, the surface of the samples was carefully polished, and the samples were mounted onto a sample tray. Then, the samples were subjected to metal coating treatment in a vacuum environment to enhance the quality of the electron microscope imaging. Through the SEM images, the microstructure of the silt reinforced by the combined MgO and EICP technology could be directly observed.

2.3.6 XRD test

In the X-ray diffraction (XRD) experiment, the samples were precisely positioned on a rotating sample stage, and as the detector rotated to specific angles, the device synchronously recorded the intensity peaks of the X-rays, generating waveform charts that visually display the crystalline structure characteristics of the samples. XRD analysis was conducted using a D8 ADVANCE diffractometer (Bruker, Germany), scanning from 10° to 90° (2θ) at a rate of 10°/min. This analysis not only involves phase identification but also focuses on the carbonate content produced under different treatment conditions and the structural differences. By analyzing the carbonate content in different samples, this study explores the correlation between the amount of carbonate produced and the reinforcement effect on the silt, thereby evaluating the effectiveness of each reinforcement technique.

3. Results and discussion

3.1 Mechanical properties analysis

To visually demonstrate the effect of the EICP and EICP-MgO systems on the reinforcement of silt, the mechanical properties of the reinforced silt were first analyzed. Fig. 5 shows the stress-strain curves and failure modes under three typical conditions: untreated samples, EICP treatment with a 3 mol/L cementation solution, and the combined treatment of 18% MgO and 3 mol/L cementation solution. The stress-strain curve of the untreated silt sample shows a rapid decline after reaching the peak, with a low peak stress (around 200 kPa), indicating weak resistance to failure. The failure mode of the untreated silt sample shows early crack formation with pronounced through-cracks. After EICP treatment, the peak stress of the sample was significantly higher than the untreated sample, reaching approximately 1200 kPa, indicating that EICP significantly improved the compressive strength of the silt. Compared to the untreated sample, the stress-strain curve of the EICP-treated sample declines more steeply after the peak, indicating increased brittleness. The failure mode shows that the EICP-treated sample developed cracks along multiple failure planes, with improved cohesion and integrity, although through-cracks still appeared. Under the combined treatment of 18% MgO and 3 mol/L cementation solution, the peak stress of the sample was significantly higher than the other treatments, reaching approximately 5137 kPa, indicating that the combination of MgO and EICP yielded the best strength enhancement in the silt. The stress-strain curve for this treatment showed a steeper decline after the peak, indicating greater brittleness. The failure mode revealed that the combined treatment resulted in cracks that penetrated the entire sample, showing typical splitting failure characteristics.

Figs. 6(a)-6(d) illustrates the effect of three different cementation solution concentrations (1 mol/L, 2 mol/L, 3 mol/L) combined with varying MgO contents (0%, 6%,

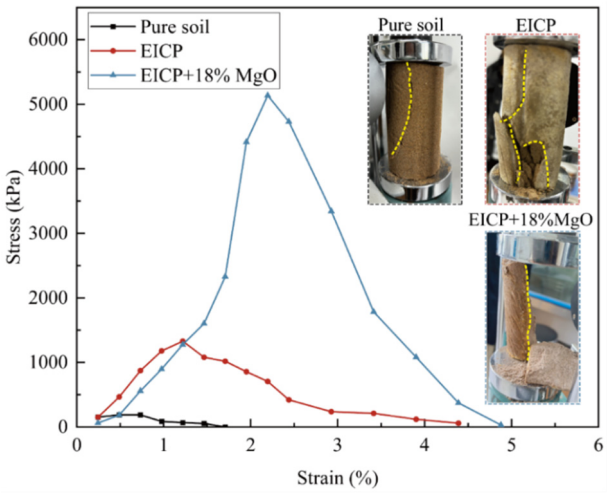

Fig. 5 Stress-strain curves and failure modes of samples with pure soil, EICP and MgO combined with EICP

10%, 14%, 18%) on four mechanical properties of the silt samples: failure strain, residual strength, elastic modulus at 50% UCS, and peak strength. Fig. 6(a) shows the trend in failure strain of the reinforced samples under different MgO contents and cementation solution concentrations. The failure strain of all reinforced soil samples reached a maximum at 6% MgO content. Low concentration cementation solution at medium MgO content (6%) significantly increased the failure strain. Fig. 6(b) shows the effect of different cementation solution concentrations and MgO contents on the residual strength of the samples. Residual strength increased with increasing MgO content under all treatment conditions. Higher concentrations of cementation solution, particularly 3 mol/L, combined with MgO, significantly improved the residual strength, indicating that the interaction between MgO and calcium carbonate effectively enhances residual strength. Fig. 6(c) displays the changes in the elastic modulus at 50% UCS under different combinations of cementation solution concentrations and MgO contents. Overall, the elastic modulus increased with rising MgO content, particularly in the combinations of high cementation solution concentration and high MgO content. This is because the magnesium carbonate hydroxide generated from the reaction of MgO with CO_3^{2-} increased the bonding between particles, reduced porosity, and enhanced the elastic modulus and deformation resistance of the samples. Fig. 6(d) shows the effect of different cementation solution concentrations and MgO contents on the peak strength of the samples. In general, the peak strength significantly increased with the rising MgO content, reaching a maximum of 5137 kPa under the combination of 3 mol/L cementation solution and 18% MgO, indicating that the synergistic effect of high cementation solution concentration and MgO markedly enhances strength.

It is noteworthy that at 6% MgO content, the unconfined compressive strength of the sample was lower than that of the EICP reinforced sample without MgO. This is because the amount of calcium carbonate and magnesium carbonate hydroxide generated was insufficient, and although Mg(OH)2 provided some bonding and filling, it was not enough to compensate for the strength loss. However, when the MgO content increased to 10%, the strength significantly exceeded that of the EICP treated sample. At this point, the effects of $Mg(OH)_2$ and magnesium carbonate hydroxide compensated for the reduction in calcium carbonate. The $Mg(OH)_2$ produced from the hydration of MgO provided weak bonding, and the hydration process increased the volume by absorbing water, filling the voids in the silt (Liang *et al.* 2018). At a relatively low dosage (6%), the hydration of MgO is limited and only a small amount of $Mg(OH)_2$ is formed, whereas higher dosages provide sufficient MgO to undergo hydration and participate in subsequent carbonation, leading to a more pronounced reinforcement effect.

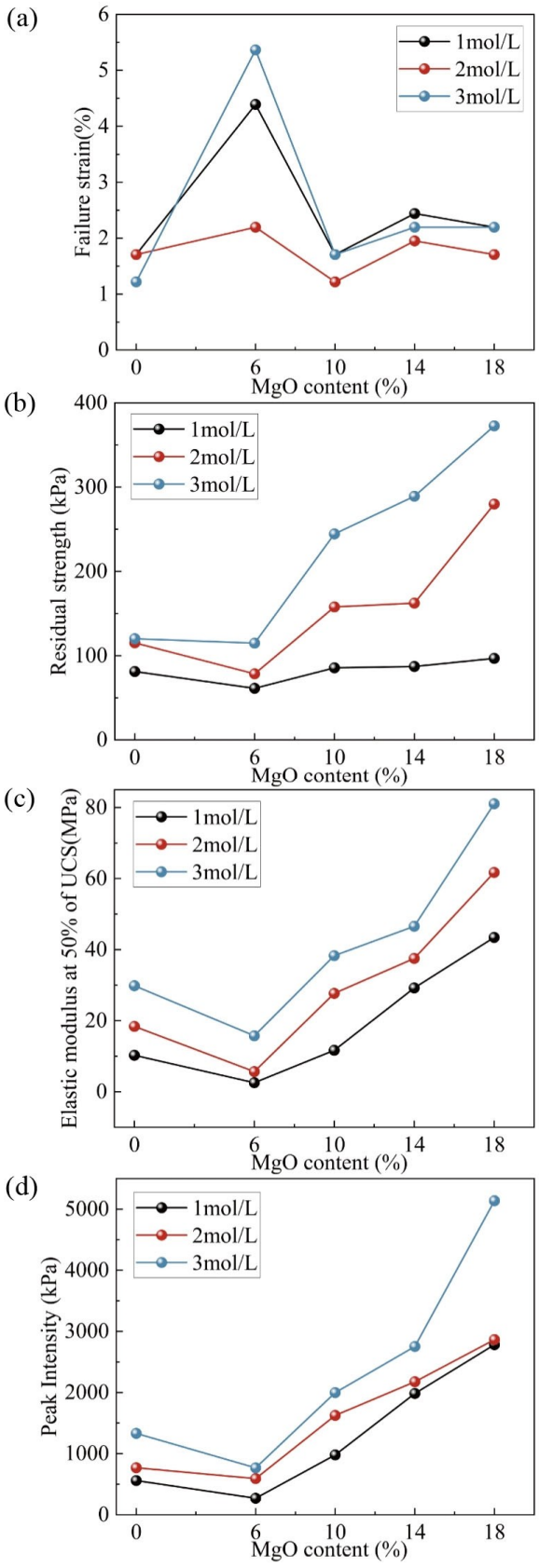

Fig. 6 Mechanical properties of silt reinforced with varying cementation solution concentrations and MgO content: (a) Failure strain, (b) Residual stress, (c) Elastic modulus at 50% unconfined strength and (d) Unconfined peak strength

3.2 Carbonate content analysis

To better understand the differences in silt reinforcement effects under various conditions, it is crucial to study the

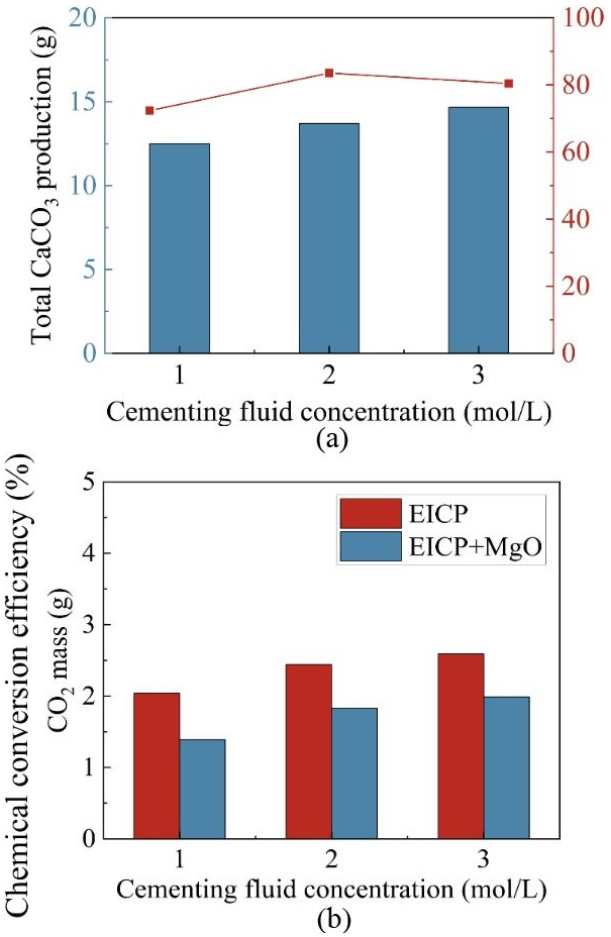

Fig. 7 Carbonate test results: (a) $CaCO_3$ production and conversion efficiency and (b) CO_2 production

contribution of carbonate production to the reinforcement effect. In the EICP process, the concentration of the cementation solution is a key factor influencing the soil reinforcement effect. Fig. 7(a) shows the trends in calcium carbonate conversion efficiency and total production under different cementation solution concentrations. As the cementation solution concentration increases, the conversion efficiency of calcium carbonate first rises and then falls, while the total amount of calcium carbonate produced continues to increase. At lower cementation solution concentrations, the increase in concentration provides more urea and calcium ions to the solution, accelerating the EICP reaction and promoting calcium carbonate precipitation (Yang and Zhao 2019). However, at higher concentrations, the excess calcium chloride inhibits urease activity, leading to a decrease in calcium carbonate conversion efficiency. Despite this, the higher concentration reactions still produced more calcium carbonate precipitates. The trend in calcium carbonate production is consistent with the changes in sample strength, further validating the correlation between calcium carbonate production and strength enhancement (Mujah *et al*. 2017).

Since the addition of MgO leads to the formation of magnesium carbonate hydroxide and basic magnesium carbonates, focusing only on calcium carbonate precipitation underestimates the total carbonate production and its contribution to soil reinforcement. In this case, CO_2 production is used to measure the overall carbonate production. Fig. 7(b) shows the CO_2 production in solution under pure EICP and combined EICP-MgO conditions. The results indicate that although the total calcium carbonate production in the EICP–MgO system is lower than in the EICP-only system, the formation of $Mg(OH)_2$ and basic magnesium carbonates provides additional bonding and pore-filling effects. These products contribute significantly to strength enhancement, explaining why the EICP–MgO method achieves superior reinforcement performance despite reduced $CaCO_3$ precipitation. This suggests that the addition of MgO causes some CO_3^{2-} to combine with magnesium ions, forming magnesium carbonate hydroxide. These additional magnesium carbonate hydrates, together with $Mg(OH)_2$, act as effective binders that fill pores and provide structural reinforcement. The addition of MgO not only enhances the bonding effect of the soil by generating $Mg(OH)_2$ but also fills the pores, improving the overall structural stability. Therefore, although the amount of calcium carbonate produced decreases, the contribution of $Mg(OH)_2$ may result in a reinforcement effect that is comparable to, or even superior to, using EICP alone. This highlights that the improvement mechanism in the combined system relies more on the synergistic action of multiple carbonate phases rather than on carbonate mass alone. This demonstrates that in the combined EICP-MgO application, it is necessary to consider the combined effects of $Mg(OH)_2$ and basic carbonates on the microstructure of the soil when evaluating the reinforcement effect, rather than focusing solely on the total carbonate production.

3.3 Calcium-induced flocculation process analysis

The improvement in mechanical properties is closely related to the formation of carbonates during the reinforcement process, making it necessary to further investigate the calcification and flocculation processes in both the EICP and EICP-MgO systems. Fig. 8 shows a comparison of the flocculation and sedimentation times between the two systems during the reaction. In the first 5 minutes of the reaction, the EICP system exhibited rapid flocculation, while the EICP-MgO system only began to show signs of flocculation at around 30 minutes, indicating that the presence of MgO delayed the onset of flocculation. This delay may be due to the slower dissolution rate of MgO, which initially did not significantly alter the chemical properties of the solution. By 30 minutes, flocculation in the EICP system had significantly intensified, while the EICP-MgO system only showed noticeable flocculation effects at around 60 minutes. Although the flocculation process in the EICP-MgO system was slower, the formation of magnesium carbonate hydroxide and $Mg(OH)_2$ contributed to improved density and stability of the later-stage sediment.

As the reaction progressed, the EICP system showed a significant increase in sedimentation at 180 minutes, with the solution gradually becoming clear. In contrast, the EICP-MgO system did not achieve a similar sedimentation effect until 360 minutes. Despite the slower reaction rate,

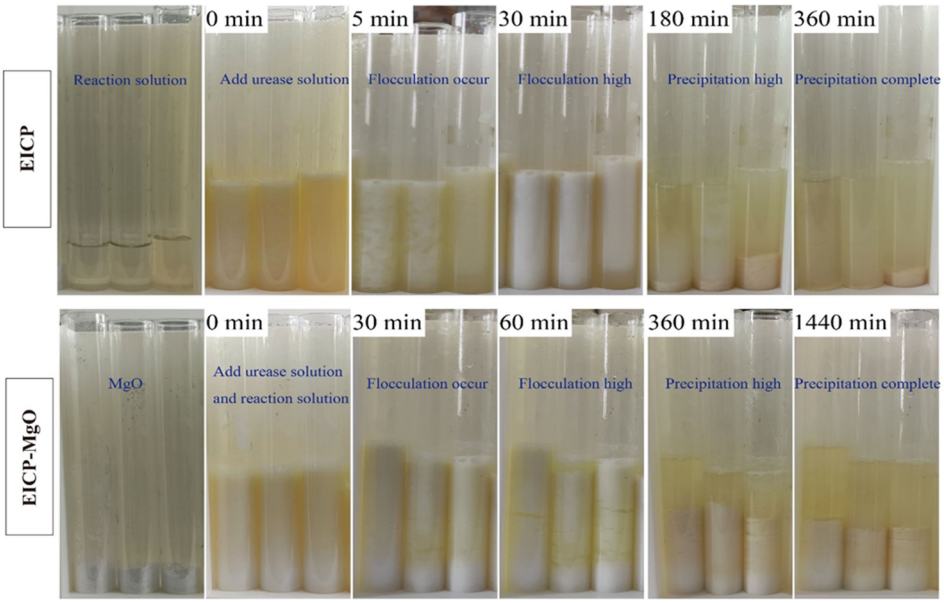

Fig. 8 EICP and EICP-MgO flocculation process

the sedimentation in the EICP-MgO system was more stable, and the reinforcement effect was more pronounced. At the final observation time point, the EICP system had completely settled by 360 minutes, with the solution becoming fully transparent. The EICP-MgO system, however, required up to 1440 minutes to achieve complete sedimentation, with a sedimentation volume that was significantly greater than that of the EICP system. Although the addition of MgO slowed the reaction rate, it significantly increased flocculation and sedimentation, thereby enhancing the apparent precipitation and pore-filling effect. This is attributed to the formation of $Mg(OH)_2$ and basic magnesium carbonates, which contribute to soil stabilization even though the total $CaCO_3$ precipitation is reduced. This is because MgO generated $Mg(OH)_2$ and basic carbonates in the EICP solution. Additionally, the different concentrations of cementation solution had a minimal impact on the flocculation and sedimentation process, indicating that the sedimentation process was primarily controlled by the reaction time of MgO, rather than the concentration of the cementation solution.

3.4 Microstructure analysis

SEM microstructure analysis can reveal the distribution of reinforcing components within the soil and their role in enhancing the reinforcement effect. Figs. 9(a), 9(c), and 9(e) show the microstructure of silt reinforced by EICP after uniaxial compression failure under cementation solution concentrations of 1 mol/L, 2 mol/L, and 3 mol/L, respectively. Under the low concentration of 1 mol/L cementation solution, the reaction was incomplete, and the resulting vaterite (spherical) particles were small, with multiple cracks visible. Due to the low concentration, calcium carbonate was unable to effectively bridge the particles, leading to a higher porosity and poorer strength and mechanical performance of the sample. As the cementation solution concentration increased (2 mol/L and 3 mol/L), the amount of calcite (rhombohedral) gradually increased, and the inter-particle porosity was significantly reduced, showing tighter particle bonding and bridging, which improved the mechanical strength of the sample. This change in microstructure is consistent with the trend observed in unconfined compressive strength, further validating the significant influence of cementation solution concentration on the EICP reinforcement effect.

Figs. 9(b), 9(d), and 9(f) show the microstructure of reinforced silt with MgO contents of 6%, 10%, and 18%, respectively. When the MgO content was 6%, a significant amount of $Mg(OH)_2$ formed on the sample surface, partially filling the pores and reducing fracture phenomena. However, due to the low strength of $Mg(OH)_2$, the overall reinforcement effect was not significant. As the MgO content increased to 10% and 18%, the amount of magnesium carbonate hydroxide in the sample increased, forming a large number of carbonation products. The identification of nesquehonite and hydromagnesite was based on characteristic diffraction peaks in the XRD spectra (Fig. 10(b)), which matched standard reference patterns, and was further supported by SEM morphology. Previous studies have also shown that nesquehonite can transform into hydromagnesite under changing external conditions, with both phases exhibiting strong cementing properties (Unluer and Al-Tabbaa 2014). These carbonation products effectively filled the inter-particle pores and bridged the particles, significantly improving the density and mechanical performance of the samples. This finding is consistent with Cai *et al*. (2017), who demonstrated that carbonation products can encapsulate and bond particles, filling voids in the soil during active MgO carbonation reinforcement. This also aligns with the results of the unconfined compressive strength tests, showing that the higher the MgO content, the greater the strength and the more pronounced the reinforcement effect.

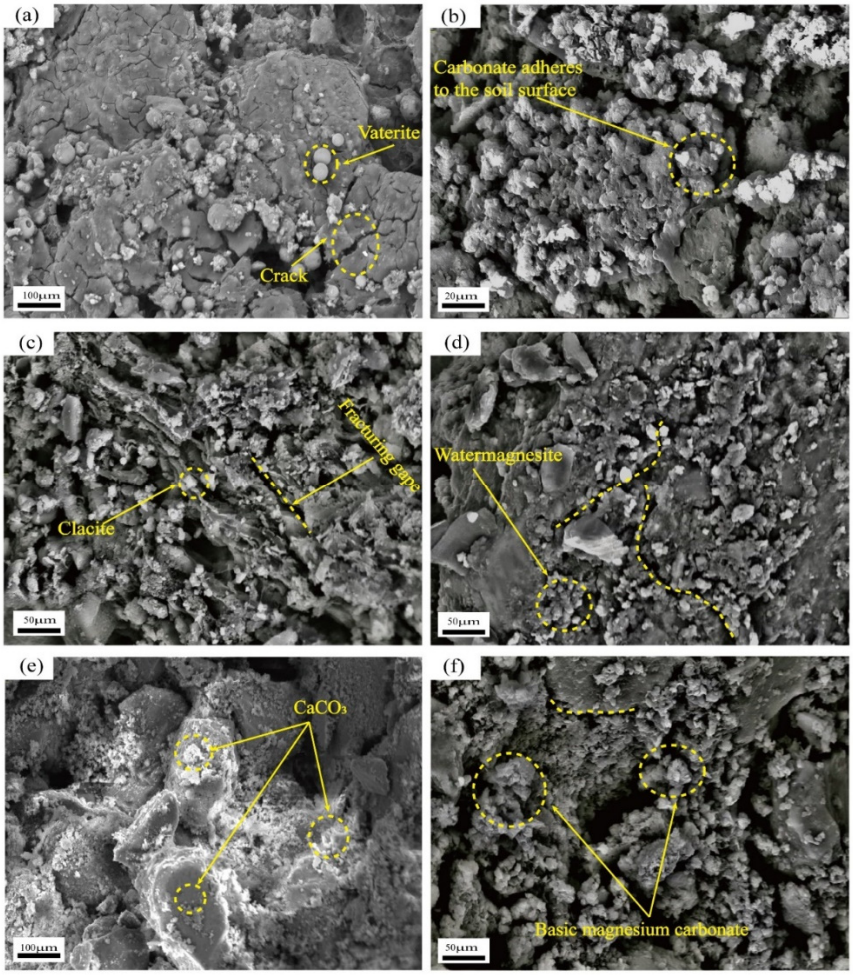

Fig. 9 SEM results of different cementing fluid concentrations and MgO content: (a) 1 mol/L solution, 0% MgO, (b) 3 mol/L solution, 6% MgO, (c) 2 mol/L solution, 0% MgO, (d) 3 mol/L solution, 10% MgO, (e) 3 mol/L solution, 0% MgO and (f) 3 mol/L solution, 18% MgO

3.5 Mineral composition analysis

To clarify the mineral composition of the reinforced silt under different reinforcement conditions, XRD analysis was conducted on the resulting mineral components to better understand the contribution of various minerals to the soil structure. Figs. 10(a) and 10(b) present the XRD results of silt reinforced by EICP and EICP-MgO at different cementation solution concentrations. The XRD spectra show that quartz remains the primary component in the silt after all reinforcement treatments. In the samples reinforced with only EICP, the peak intensity of calcium carbonate increases with the concentration of the cementation solution, and significant calcium carbonate crystals were observed through SEM.

When MgO was added, the calcium carbonate content at low MgO levels was lower than in samples reinforced with only EICP. This is because MgO initially inhibited urease activity, reducing calcium carbonate formation. As the MgO content increased, peaks for $Mg(OH)_2$ and basic magnesium carbonates (such as hydromagnesite and nesquehonite) appeared in the XRD spectra, enriching the mineral composition. However, since the $Mg(OH)_2$ was not fully carbonated, its peak intensity increased with higher MgO content, while the peaks for nesquehonite and hydromagnesite remained relatively weak. This indicates that at higher MgO contents, both calcium carbonate and $Mg(OH)_2$ contribute to the reinforcement. These results are consistent with the trends observed in unconfined compressive strength and microstructure, further validating the critical role of MgO in the EICP reinforcement process. It not only increases the diversity of precipitates but also significantly improves the mechanical properties of the soil.

3.6 EICP cementation process of silt particles

To understand the EICP reinforcement process at the microscale, it is necessary to observe and document the evolution of cementation between soil particles. Fig. 11 illustrates the progressive development of EICP cementation between silt particles from the Yellow River floodplain. Within the first 0 to 10 minutes, the reaction between the cementation solution and urease generates a small amount of calcium carbonate precipitate, causing an initial shift in particle positions. However, the amount of precipitate is limited, mainly due to the gradual release of

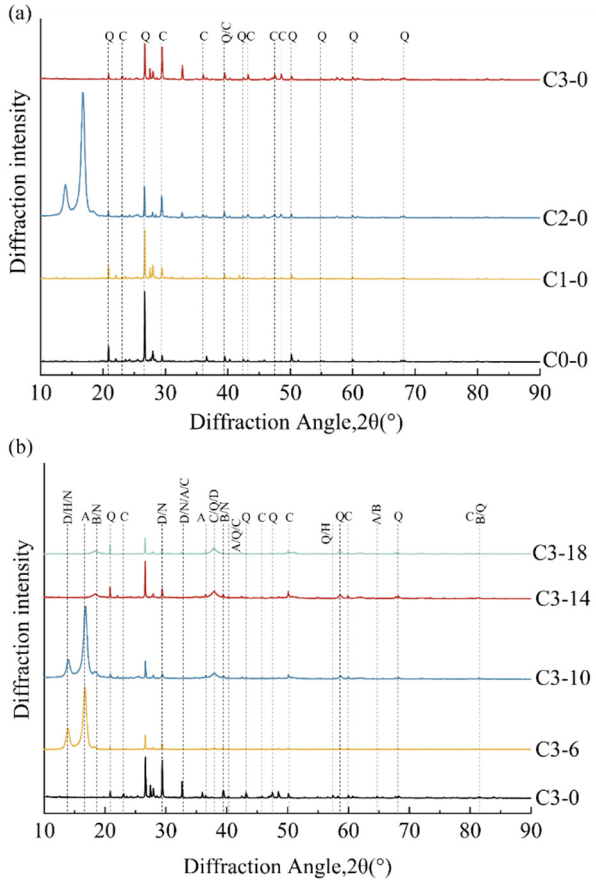

Fig. 10 XRD Results Analysis: (a) EICP XRD Results Analysis (b) EICP-MgO XRD Results Analysis

urease activity and the short reaction time. By 30 minutes, the calcium carbonate content increases, enhancing the interaction between particles, and the bridging effect begins to appear, resulting in closer contact between particles. At 60 minutes, the pores between particles are significantly reduced, and the arrangement becomes denser as more calcium carbonate precipitates, further promoting particle bonding. By 90 minutes, the calcium carbonate precipitates effectively fill the pores, with particle gaps narrowing significantly, exhibiting pore-filling cementation, where calcium carbonate fills the micro-pores. At 180 minutes, the calcium carbonate gradually encapsulates the soil particles, enhancing overall stability. By 600 minutes, the encapsulation effect becomes more pronounced, forming a stronger cementation. At 720 minutes, the cementation process is nearly complete, and by 1440 minutes, the cementation reaches a fully stabilized state, with no significant changes observed in the images, indicating maximum particle structural stability.

3.7 EICP-MgO cementation process of silt particles

After understanding the reinforcement process of EICP on silt particles, it is necessary to further study the micro-evolution of the combined EICP-MgO reinforcement process to reveal the mechanism of MgO. Fig. 12 illustrates the cementation process of the combined EICP-MgO in the silt from the Yellow River floodplain. At 10 minutes into the experiment, a small amount of calcium carbonate precipitate begins to form, consistent with the early trend observed in the EICP only process, indicating that the cementation at this stage mainly relies on urease-catalyzed calcium carbonate precipitation, with the effect of MgO not yet evident. By 30 minutes, calcium carbonate precipitation gradually increases and begins to bond the soil particles. At 60 minutes, MgO gradually dissolves and expands, reacting with the solution to form $Mg(OH)_2$ and magnesium carbonate hydroxide, significantly increasing the amount of carbonate precipitates. These precipitates encapsulate and fill the pores between the particles, and the reinforcement effect of MgO starts to become apparent.

By 90 minutes, the produced carbonates further cement the particles, strengthening the inter-particle connections. At 120 minutes, the amount of carbonate precipitates continues to increase, and the connections between particles become tighter, demonstrating an enhanced effect of both calcium carbonate and magnesium carbonate, which is more pronounced compared to EICP reinforcement alone. By 180 minutes, the pores are significantly reduced, and the cementing effect of the carbonates is further strengthened. At 720 minutes, the reaction between MgO and the cementation solution is nearly complete, with minimal changes in pore size, and the cementation effect of the precipitates stabilizes. By 1440 minutes, the carbonate precipitates, together with the increased $Mg(OH)_2$ and magnesium carbonate hydroxides formed at higher MgO dosages, fully filled the pores and bonded the particles, significantly enhancing the structural stability of the soil. The cementation process is essentially complete, and the mechanical connections reach their maximum strength. This result indicates that the combined EICP-MgO reinforcement technique significantly improves the mechanical performance of the silt from the Yellow River floodplain. Compared to EICP reinforcement alone, the addition of MgO increases the amount of precipitates and enhances the cementation effect, offering a notable reinforcement advantage.

3.8 EICP-MgO combined reinforcement mechanism

Based on the above experimental results, the mechanism of MgO-EICP reinforcement can be summarized and systematically analyzed to reveal the intrinsic mechanisms that enhance the reinforcement effect. Figs. 13(a) and 13(b) illustrate the mechanistic process of EICP reinforcement and the synergistic reinforcement of EICP-MgO in the silt from the Yellow River floodplain. During the EICP reinforcement process, CO_3^{2-} ions produced by urease-catalyzed urea hydrolysis react with Ca^{2+} to form calcium carbonate precipitates, which cement the soil particles, reduce porosity, and enhance inter-particle connections, thereby increasing the soil's strength.

The combined reinforcement process of MgO and EICP involves several key reactions. First, after MgO is evenly mixed with the silt, water in the EICP solution reacts with MgO to produce $Mg(OH)_2$. Simultaneously, CO_3^{2-} ions from urea hydrolysis react with Ca^{2+} to form calcium carbonate precipitates, further cementing the soil particles. $Mg(OH)_2$ then reacts with CO_3^{2-} to produce magnesium

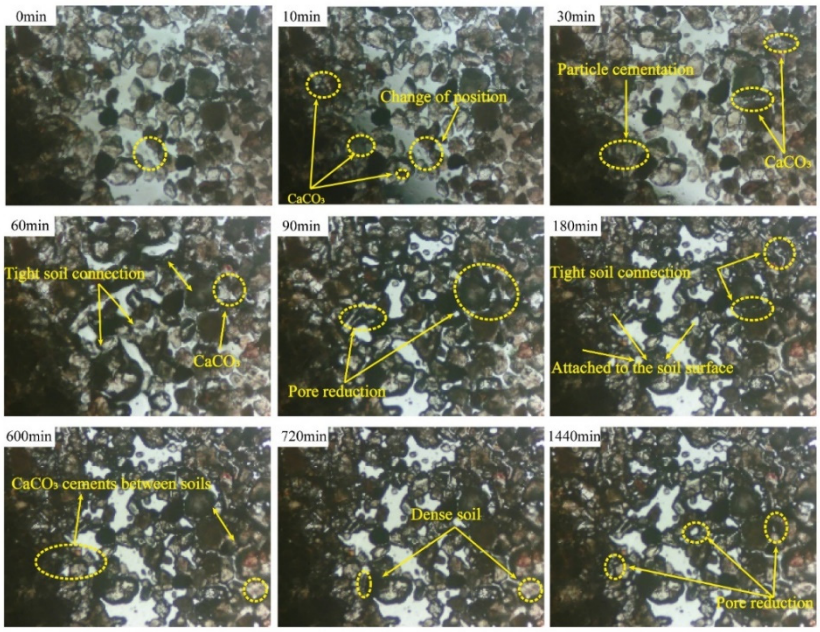

Fig. 11 Mesoscopic process diagram of EICP reinforced silt particles reinforcement mechanism

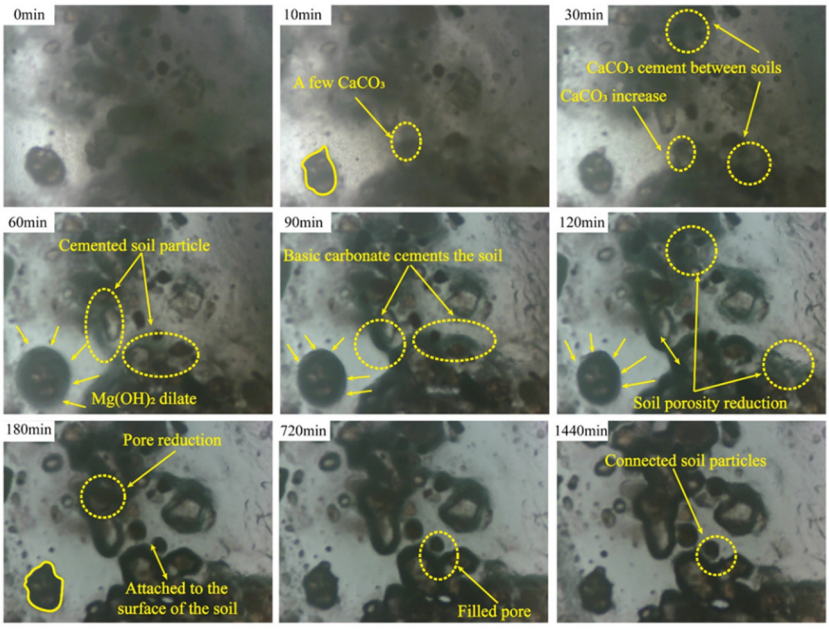

Fig. 12 Particle–pore scale process diagram of EICP-MgO reinforcement of silt particles

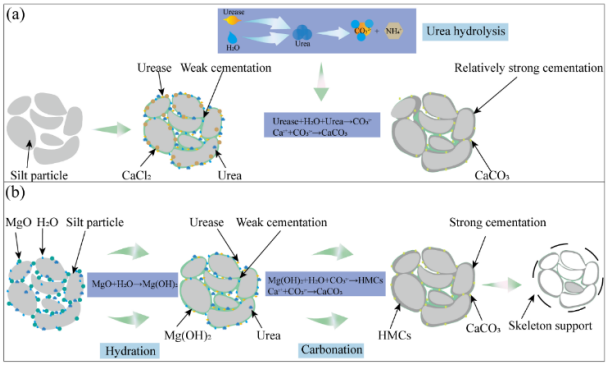

Figs. 13 Reinforcement mechanism of silt: (a) EICP reinforcement mechanism; (b) EICP-MgO combined

carbonate hydroxide. Both of these carbonates are expansive and have strong cementing properties, effectively filling the inter-particle pores and enhancing particle bonding. The synergistic action of calcium carbonate and magnesium carbonate hydroxide not only improves the structural stability of the silt but also exhibits a stronger cementation effect compared to calcium carbonate alone. Therefore, samples reinforced with EICP-MgO demonstrate significantly enhanced unconfined compressive strength, validating the effectiveness of this technique in improving the mechanical properties of the soil.

4. Conclusions

This study investigated the mechanical properties of silt from the Yellow River floodplain reinforced with the combined use of EICP and MgO, analyzing the reinforcement effects under different cementation solution concentrations and MgO contents. Through microscopy experiments, flocculation tests, and SEM analysis, the study explored the evolution process and reinforcement mechanism of EICP and EICP-MgO in reinforcing silt from the Yellow River floodplain, providing a new approach for reinforcing silt in this region. The main conclusions are as follows:

(1) In the EICP process, the conversion efficiency of calcium carbonate first increased to about 65% and then declined at higher concentrations, while the total precipitation mass rose steadily from approximately 2.5% to 6.8%. With the addition of MgO, part of the carbonate combined with magnesium to form carbonate hydrates, and together with $Mg(OH)_2$, these phases enhanced soil strength even though the yield of calcium carbonate was reduced.

(2) The unconfined compressive strength of untreated silt was only about 200 kPa. After reinforcement by the combined EICP–MgO method, the strength reached nearly 5000 kPa, which is about three times higher than samples treated with EICP alone. This demonstrates a strong synergistic effect, accompanied by improvements in residual strength and stiffness.

(3) In the flocculation and sedimentation tests, the EICP–MgO system flocculated more slowly but ultimately produced 20 to 30 percent more sediment than the EICP system. This shows that MgO addition delays the early reaction but increases the final amount of precipitation.

(4) Scanning electron microscopy revealed that the porosity of the samples decreased from roughly 35 percent to 22 percent as the concentration of the cementation solution increased. When the MgO dosage was in the range of 12 to 18 percent, additional bonding phases such as $Mg(OH)_2$ and magnesium carbonate hydrates appeared, producing a much denser soil structure.

(5) X-ray diffraction confirmed that calcium carbonate in the EICP system gradually transformed from vaterite to calcite, which improved mechanical stability. In the combined system, magnesium carbonate hydrates became the dominant phase, further tightening the interparticle bonding and reinforcing the soil structure.

Overall, the combined EICP and MgO reinforcement method is a highly promising green soil reinforcement technology that can effectively improve the mechanical properties of silt. It offers a practical and efficient alternative to traditional soil reinforcement techniques. Nevertheless, this study was limited to laboratory-scale tests on reconstituted silt specimens with a fixed soybean urease concentration. Future research should evaluate long-term durability, field-scale applicability, and the effects of varying urease concentrations and curing conditions. Furthermore, systematic investigation of the coupled precipitation–carbonation mechanisms will provide deeper insights into the synergy between EICP and MgO.

Acknowledgments

This work was supported by the Henan Provincial Natural Science Foundation of China (222300420174), Natural Science Foundation of China (42402184), the China Postdoctoral Science Foundation (2021M701097) and Key Projects of the Universities in Henan Province (23A170006).

References

Achal, V. and Mukherjee, A. (2015), "A review of microbial precipitation for sustainable construction", *Constr. Build. Mater.*, **93**(1), 1224-1235. https://doi.org/10.1016/j.conbuildmat.2015.04.051.

Almajed, A., Tirkolaei, H.K., Kavazanjian Jr, E. and Hamdan, N. (2019), "Enzyme induced biocementated sand with high strength at low carbonate content", *Sci. Rep.*, **9**(1), 1135. https://doi.org/10.1038/s41598-018-38361-1.

Cai, G.H., Liu, S.Y. and Cao, J.J. (2017), "Research on micro-mechanism of carbonated reactive MgO-stabilized silt", *Chin. Civ. Eng. J.*, **50**(1), 105-113.

Chen, Y., Han, Y., Zhang, X., Sarajpoor, S., Zhang, S. and Yao, X. (2023), "Experimental study on permeability and strength characteristics of MICP-treated calcareous sand", *Biogeotechnics*, **1**(3), 100034. https://doi.org/10.1016/j.biogeo.2023.100034.

Chen, Z., Fang, X., Long, K., Shen, C., Yang, Y. and Liu, J. (2021), "Using the biocarbonization of reactive magnesia to cure electrolytic manganese residue", *Geomicrobiol. J.*, **38**(8), 709-718. https://doi.org/10.1080/01490451.2021.1939812.

DeJong, J.T., Fritzges, M.B. and Nüsslein, K. (2006), "Microbially induced cementation to control sand response to undrained shear", *J. Geotech. Geoenviron. Eng.*, **132**(11), 1381-1392. https://doi.org/10.1061/(ASCE)1090-0241(2006)132:11(1381).

DeJong, J.T., Mortensen, B.M., Martinez, B.C. and Nelson, D.C. (2010), "Bio-mediated soil improvement", *Ecol. Eng.*, **36**(2), 197-210. https://doi.org/10.1016/j.ecoleng.2008.12.029.

Dung, N.T., Hoang, T., Yang, E.H., Chu, J. and Unluer, C. (2022), "New frontiers in sustainable cements: Improving the performance of carbonated reactive MgO concrete via microbial carbonation process", *Constr. Build. Mater.*, **356**(1), 129243. https://doi.org/10.1016/j.conbuildmat.2022.129243.

Gao, Y., He, J., Tang, X. and Chu, J. (2019), "Calcium carbonate precipitation catalyzed by soybean urease as an improvement method for fine-grained soil", Soils Found., 59(5), 1631-1637. https://doi.org/10.1016/j.sandf.2019.03.014.

Harianto, T., Hayashi, S., Du, Y.J. and Suetsugu, D. (2008), "Effects of fiber additives on the desiccation crack behavior of the compacted Akaboku soil as a material for landfill cover barrier", *Water Air Soil Pollut.*, **194**(1), 141-149. https://doi.org/10.1007/s11270-008-9703-2.

He, J., Fang, C., Hang, L., Qi, Y., Mao, X., Yan, B., Zhou, Y. and Gao, Y. (2021), "Enzyme induced carbonate precipitation for soil internal erosion control under water seepage", *Geomech. Eng.*, **26**(3), 289-299. https://doi.org/10.12989/gae.2021.26.3.289.

Huang, F. (2020), "Review on the application of microbial mineralization technology in large-scale soil improvement", *Henan Sci. Technol.*, **39**(1), 95-101.

Huang, T., Fang, X., Zhang, W., Shen, C. and Lei, Y. (2020), "Experimental study on solidified loess by microbes and reactive magnesium oxide", *Rock Soil Mech.*, **41**(11), 3300-3306.

Ibraim, E., Diambra, A., Russell, A.R. and Wood, D.M. (2012), "Assessment of laboratory sample preparation for fibre reinforced sands", *Geotext. Geomembranes*., 34(1), 69-79. https://doi.org/10.1016/j.geotexmem.2012.03.002.

Jin, Q., Zheng, Y., Cui, X., Cui, S., Qi, H., Zhang, X. and Wang, S. (2020), "Evaluation of dynamic characteristics of silt in Yellow River flood field after freeze-thaw cycles", *J. Cent. South Univ*., **27**(7), 2113-2122. https://doi.org/10.1007/s11771-020-4434-7.

Kavazanjian, E. and Hamdan, N. (2015), "Enzyme induced carbonate precipitation (EICP) columns for ground improvement", *Proceedings of the IFCEE 2015*, San Antonio, TX, March. https://doi.org/10.1061/9780784479087.209.

Kavazanjian Jr, E., Almajed, A. and Hamdan, N. (2017), "Bio-inspired soil improvement using EICP soil columns and soil nails", Grouting 2017, Honolulu, HI, July.

Khoshdel Sangdeh, M., Salimi, M., Khansar, H.H., Dokaneh, M., Ranjbar, P.Z., Payan, M. and Arabani, M. (2024), "Predicting the precipitated calcium carbonate and unconfined compressive strength of bio-mediated sands through robust hybrid optimization algorithms", *Transport. Geotech*., **46**, 101235. https://doi.org/10.1016/j.trgeo.2024.101235.

Khattak, M.J. and Alrashidi, M. (2006), "Durability and mechanistic characteristics of fiber reinforced soil–cement mixtures", *Int. J. Pavement Eng*., **7**(1), 53-62. https://doi.org/10.1080/10298430500489207.

Li, X., Li, S., Yao, K., Zhu, S. and Lv, G. (2011), "Test study of changing rules of excess pore water pressure during dynamic consolidation at subgrade of expressway in Yellow River flood area", *Rock Soil Mech*., **32**(9), 2815-2820.

Liang, W., Liu, S., Cai, G. and Tang, H. (2018), "Permeability properties of carbonated reactive MgO-stabilized soils", *Chin. J. Geotech. Eng*., **40**(6), 953-959.

Liu, K., Jiang, N., Qin, J., Wang, Y., Tang, C. and Han, X. (2021), "An experimental study of mitigating coastal sand dune erosion by microbial- and enzymatic-induced carbonate precipitation", *Acta Geotech*., **16**(2), 467-480. https://doi.org/10.1007/s11440-020-01046-z.

Liu, S. and Li, C. (2015), "Influence of MgO activity on stabilization efficiency of carbonated mixing method", *Chin. J. Geotech. Eng*., **37**(2), 148-155.

Meng, H., Shu, S., Gao, Y., Yan, B. and He, J. (2021), "Multiple-phase enzyme-induced carbonate precipitation (EICP) method for soil improvement", *Eng. Geol*., **294**(1), 106374. https://doi.org/10.1016/j.enggeo.2021.106374.

Morales, L., Garzón, E., Romero, E. and Sánchez-Soto, P.J. (2019), "Microbiological induced carbonate precipitation using clay phyllites to replace chemical stabilizers", *Appl. Clay Sci*., **174**(1), 15-28. https://doi.org/10.1016/j.clay.2019.03.018.

Mujah, D., Shahin, M.A. and Cheng, L. (2017), "State-of-the-art review of biocementation by microbially induced calcite precipitation (MICP) for soil stabilization", *Geomicrobiol. J*., **34**(6), 524-537. https://doi.org/10.1080/01490451.2016.1225866.

Nafisi, A., Safavizadeh, S. and Montoya, B.M. (2019), "Influence of microbe and enzyme-induced treatments on cemented sand shear response", *J. Geotech. Geoenviron. Eng*., **145**(6), 06019008. https://doi.org/10.1061/(ASCE)GT.1943-5606.0002111.

Payan, M., Khoshdel Sangdeh, M., Salimi, M., Ranjbar, P.Z., Arabani, M. and Hosseinpour, I. (2024), "A comprehensive review on the application of microbially induced calcite precipitation (MICP) technique in soil erosion mitigation as a sustainable and environmentally friendly approach", *Results Eng*., **24**, 103235. https://doi.org/10.1016/j.rineng.2024.103235.

Putra, H., Yasuhara, H., Kinoshita, N. and Hirata, A. (2017), "Application of magnesium to improve uniform distribution of precipitated minerals in 1-m column specimens", *Geomech. Eng*., **12**(5), 803-813. https://doi.org/10.12989/gae.2017.12.5.803.

Qi, Y., Gao, Y., Meng, H., He, J. and Liu, Y. (2022), "Biocementation via soybean-urease induced carbonate precipitation using carbide slag powder derived soluble calcium", *Geomech. Eng*., **29**(1), 79-90. https://doi.org/10.12989/gae.2022.29.1.079.

Ran, D., Watanabe, J. and Kawasaki, S. (2015), "Sand cementation test using plant-derived urease and calcium phosphate compound", *Mater. Trans*., **56**(8), 1565-1572. https://doi.org/10.2320/matertrans.M-M2015818.

Rodriguez-Navarro, C., Cazalla, O., Elert, K. and Sebastian, E. (2002), "Liesegang pattern development in carbonating traditional lime mortars", *Proc. R. Soc. Lond. A*, **458**(2028), 2261-2273. https://doi.org/10.1098/rspa.2002.0975.

Shu, S., Yan, B., Ge, B., Li, S. and Meng, H. (2022), "Factors affecting soybean crude urease extraction and biocementation via enzyme-induced carbonate precipitation (EICP) for soil improvement", *Energies*, **15**(15), 5566. https://doi.org/10.3390/en15155566.

Song, J.Y., Sim, Y., Jang, J., Hong, W.T. and Yun, T.S. (2020), "Near-surface soil stabilization by enzyme-induced carbonate precipitation for fugitive dust suppression", *Acta Geotech*., **15**(6), 1967-1980. https://doi.org/10.1007/s11440-019-00881-z.

Terzis, D. and Laloui, L. (2019), "A decade of progress and turning points in the understanding of bio-improved soils: A review", *Geomech. Energy Environ*., **19**(1), 100116. https://doi.org/10.1016/j.gete.2019.03.001.

Unluer, C. and Al-Tabbaa, A. (2013), "Impact of hydrated magnesium carbonate additives on the carbonation of reactive MgO cements", *Cem. Concrete Res*., **54**(1), 87-97. https://doi.org/10.1016/j.cemconres.2013.08.009.

Unluer, C. and Al-Tabbaa, A. (2014), "Enhancing the carbonation of MgO cement porous blocks through improved curing conditions", *Cem. Concrete Res*., **59**(1), 55-65. https://doi.org/10.1016/j.cemconres.2014.02.005.

Vandeperre, L.J., Liska, M. and Al-Tabbaa, A. (2008a), "Hydration and mechanical properties of magnesia, pulverized fuel ash, and portland cement blends", *J. Mater. Civ. Eng*., 20(5), 375-383. https://doi.org/10.1061/(ASCE)0899-1561(2008)20:5(375).

Vandeperre, L., Liska, M. and Al-Tabbaa, A. (2008b), "Microstructures of reactive magnesia cement blends", *Cement Concrete Comp*., **30**(9), 706-714. https://doi.org/10.1016/j.cemconcomp.2008.05.002.

Wang, D., Tang, C., Pan, X., Wang, R., Li, J., Dong, Z. and Shi, B. (2022), "Construction and demolition waste stabilization through a bio-carbonation of reactive magnesia cement for underwater engineering", *Constr. Build. Mater*., **335**(1), 127458. https://doi.org/10.1016/j.conbuildmat.2022.127458.

Wang, H., Zhao, Z. and Zhang, T. (2016), "Performance of improved soil subgrade under freeze-thaw cycles in flood retarding basin", *J. Nanjing For. Univ*., **59**(3), 156. https://doi.org/10.3969/j.issn.1000-2006.2016.03.026.

Whiffin, V.S. (2004), "Microbial $CaCO_3$ precipitation for the production of biocement", Ph.D. Dissertation, Murdoch University, Perth, Australia.

Whiffin, V.S., Van Paassen, L.A. and Harkes, M.P. (2007), "Microbial carbonate precipitation as a soil improvement technique", *Geomicrobiol. J*., **24**(5), 417-423. https://doi.org/10.1080/01490450701436505.

Wu, L., Miao, L., Sun, X., Chen, R. and Wang, C. (2020), "Experimental study on sand solidification using plant-derived urease-induced calcium carbonate precipitation", *Chin. J. Geotech. Eng*., **42**(4), 714-720.

Xiao, Y., He, X., Evans, T.M., Stuedlein, A.W. and Liu, H. (2019), "Unconfined compressive and splitting tensile strength of basalt

fiber–reinforced biocemented sand", *J. Geotech. Geoenviron. Eng*., 145(6), 04019048. https://doi.org/10.1061/(ASCE)GT.1943-5606.0002108.

Yang, Y. and Zhao, Z. (2019), "Study on the influence of cementation solution concentration on reinforcement of marine silt by microbial grouting", *Rock Soil Mech*., **40**(7), 2525-2532.

Yang, Y., Ruan, S., Wu, S., Chu, J., Unluer, C., Liu, H. and Cheng, L. (2021), "Biocarbonation of reactive magnesia for soil improvement", *Acta Geotech*., **16**(4), 1113-1125. https://doi.org/10.1007/s11440-020-01093-6.

Yi, Y., Liska, M., Unluer, C. and Al-Tabbaa, A. (2013), "Carbonating magnesia for soil stabilization", *Can. Geotech. J*., **50**(9), 899-905. https://doi.org/10.1139/cgj-2012-0364.

Yin, L., Tang, C., Xie, Y., Lu, C., Jiang, N. and Shi, B. (2019), "Factors affecting improvement in engineering properties of geomaterials by microbial-induced calcite precipitation", *Rock Soil Mech*., **40**(8), 2525-2536.

Yuan, H., Liu, K., Zhang, C. and Zhao, Z. (2022), "Mechanical properties of Na-montmorillonite-modified EICP-treated silty sand", *Environ. Sci. Pollut. Res*., **29**(1), 1-13. https://doi.org/10.1007/s11356-021-16442-5.

Zhang, J., Wang, X., Shi, L. and Yin, Y. (2022), "Enzyme-induced carbonate precipitation (EICP) combined with lignin to solidify silt in the Yellow River flood area", *Constr. Build. Mater*., **339**(1), 127792. https://doi.org/10.1016/j.conbuildmat.2022.127792.

Zhu, L., Lang, C., Li, B., Wen, K. and Li, M. (2022), "Characteristics of soybean urease induced $CaCO_3$ precipitation", *Geomech. Eng*., **31**(3), 281-289. https://doi.org/10.12989/gae.2022.31.3.281.

CC